Frank, U., Nowaczyk, N., Negendank, J. F. (2007): Rock magnetism of greigite bearing sediments from the Dead Sea, Israel. - Geophysical Journal International, 168, 3, pp. 921—934.

DOI: http://doi.org/doi:10.1111/j.1365-246X.2006.03273.x

Geophys. J. Int. (2007) **168,** 921–934 doi: 10.1111/j.1365-246X.2006.03273.x

Rock magnetism of greigite bearing sediments from the Dead Sea, Israel

Ute Frank, Norbert R. Nowaczyk and Jörg F. W. Negendank

GeoForschungsZentrum Potsdam, Section 3.3. *Climate dynamics and sedimentation, Telegrafenberg,* D-14473 *Potsdam, Germany.*
E-mail: ufrank@gfz-potsdam.de

Accepted 2006 October 18. Received 2006 October 18; in original form 2005 September 27

SUMMARY

Laminated evaporitic sediments from the Dead Sea, Israel, were subjected to detailed rock magnetic investigations including the analysis of laboratory induced magnetizations and high temperature runs of the saturation magnetization. Ti-magnetite and greigite were identified as the main magnetic carrier minerals. The variations in concentration, grain size and coercitivity depended parameters reflect the varying amount of greigite with respect to Ti-magnetite. Samples with a high greigite concentration are characterized by *S*-ratios close to 1 in combination with low J_{ARM}/J_{SIRM} ratios. The results of a hierarchical agglomerative cluster analysis of the rock magnetic data presented in form of scatter plots allow for a qualitative identification of greigite-indicative parameters/parameter ratios and thus semi-quantitative estimation of the greigite content. The samples from the Dead Sea are distributed along a mixing line between the end members pure greigite and low Ti-magnetite. Determination of hysteresis parameters revealed that the greigite dominated samples show SD-behaviour whereas the Ti-magnetites plot in the PSD-range.

Key words: Dead Sea, greigite, Israel, lacustrine sediments, rock magnetism, Ti-magnetite.

INTRODUCTION

The main purpose of rock magnetic investigations of sediments is to identify the magnetic carrier minerals, to quantify their grain size as well as concentration variations, and to detect any kind of diagenetic overprints. The obtained information could either be used to validate any palaeomagnetic interpretation of the investigated sediments, that is, strength and direction of the geomagnetic palaeofield vector (e.g. Frank *et al.* 2007; Geiss & Banerjee 2003; Yamazaki *et al.* 2003), or to interpret the rock magnetic records in terms of climatic variations. The latter became quite popular during the last two decades, not only concentrating on the multipurpose tool magnetic susceptibility, but also using the parameters magnetic coercitivity, magnetic grain size variations and so on (e.g. Geiss & Banerjee 1997; Vlag *et al.* 1997; Wang *et al.* 2001; Hirt *et al.* 2003; Rolph *et al.* 2004). Most rock magnetic investigations focussed on sediments containing (Ti-) magnetites as the main magnetic carrier minerals, often with contributions by high coercitive minerals like goethite and hematite. However, during the last decade special emphasis was placed on studies on greigite bearing sediments, (e.g. Snowball 1991; Jansa *et al.* 1998; Reynolds *et al.* 1999; Sagnotti & Winkler 1999; Strechie *et al.* 2002; Roberts & Weaver 2005, and references therein). The number of papers on this subject is still increasing. Sedimentary sequences that have a more complex composition of the magnetic mineral fraction, like a mixture of (Ti-) magnetite and greigite throughout the whole profile, have been the subject of only a handful of detailed rock magnetic investigations so far (Roberts & Turner 1993; Snowball 1997a; Jelinowska *et al.* 1998). Because greigite is supposed to be formed during diagenesis, carrying a secondary magnetization with unknown age, these sediments are generally thought of being useless for palaeomagnetic reconstructions and climatic interpretations as well. Nevertheless, it is quite of interest for all magnetists working with sediments, especially lake sediments, to see if and how the variations in the standard rock magnetic parameters, determined as part of the normal sediment investigation routine, are linked to variations in the presence of two magnetic mineral fractions. By this way, we also obtained more information about the rock magnetic characteristics of greigite and greigite bearing sediments, like those from the western shore of the Dead Sea, Israel, presented here. The processes leading to the presence of greigite in the Dead Sea sediments and the impact of the greigite formation on the palaeomagnetic results will be discussed in Frank *et al.* (2007).

SITE LOCATION AND MATERIAL

The Dead Sea with its lake level at about 400 m below sea level is situated in a NNE–SSW stretching pull-apart basin, which formed as part of the Dead Sea-rift zone about 15 Ma ago. (Garfunkel & Ben-Avraham 1996) (Fig. 1). The graben walls at both sides of the Dead Sea basin are build up by Cretaceous carbonatic rocks in the west and sandstones in the east. Most of the clastic material brought into the lake is transported by temporarily active rivers at the western rim of the basin and by the Jordan River from the North (Fig. 1).

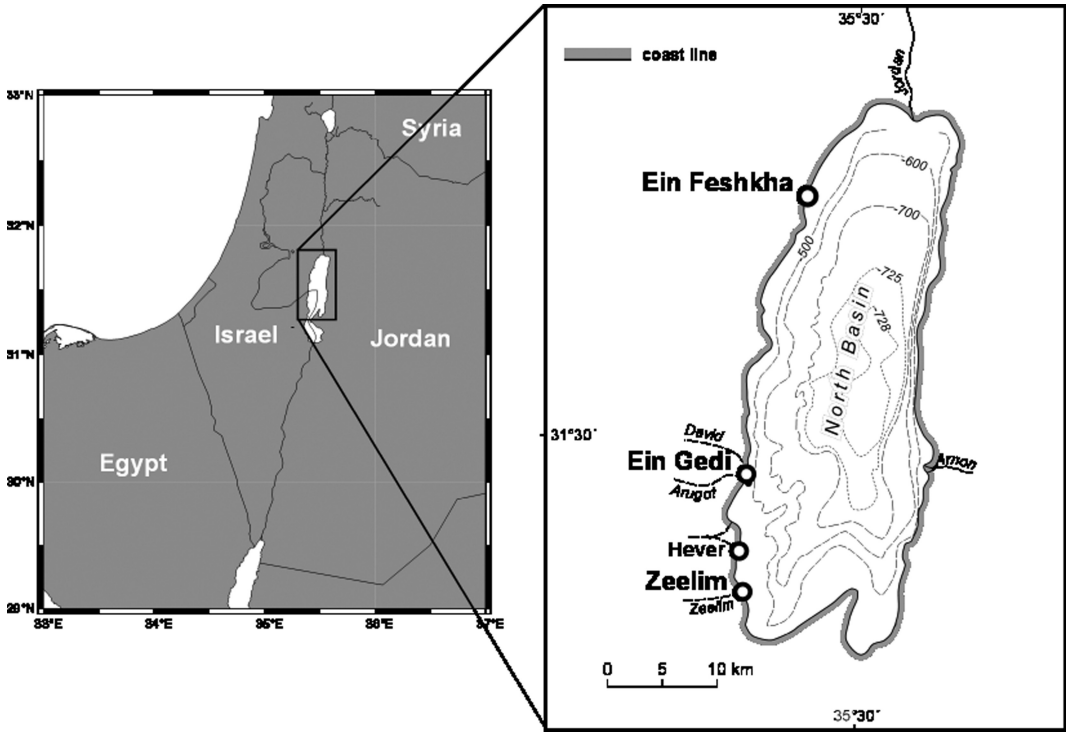

Figure 1. Location and bathymetry (mbsf) of the North Basin of the Dead Sea, Israel. The coring sites on the western shore of the Dead Sea are marked by circles.

Both fluviatile systems are forming fan delta structures at their front. Most of the primary magnetic material is supposed to be transported by the Jordan River, cutting through basaltic rocks of Quaternary age and the sediments of Lake Lisan (the palaeo-Dead Sea) on its way to the Dead Sea.

During a drilling campaign in 1997 a total of nine sediment cores with lengths between 0.6 and 19 m were recovered from four different sites on the western shore of the Dead Sea (Migowski *et al.* 1998) (Fig. 1, Table 1). Due to the rapid drop of the lake level of the Dead Sea at a rate of 32 cm a^{-1} in the last decades (Hassan & Klein 2002) the coring locations at the shore revealed complete sediment records of the former lacustrine to near shore environments during the last ca. 10 ka (Migowski *et al.* 1998). The sediments in all cores are composed of alternating fine layers of detrital material and authigenic aragonite with intercalated sand as well as salt layers of up to 2 m thickness, reflecting the variations in the lake level of the Dead Sea (Fig. 2). Thin dark layers that are present in nearly all sediment sections point to the presence of Fe-sulphides, most probably greigite, during periods of anoxic lake bottom conditions. From the material available, the five long cores DSEn-C/A and DSEn-B from Ein Gedi, DSZ-A and DSZ-B from Ze'elim and Core DSF-B from Ein Feshkha were chosen for palaeomagnetic investigations. The results will be presented elsewhere. Detailed rock magnetic investigations were carried out only on one core from each site; these are DSEn-C/A, DSZ-A and DSF-B. The core from site Hever was not investigated due to massive sediment deformation in the uppermost 150 cm and the lack of an age model.

Table 1. Overview about the sediment cores available from the four Dead sea sites including site coordinates and core length.

Site	Site coordinates	Core name	Core length (m)
Ein Feshkha	31°42′N, 35°27′E	DSF-A	2.62
		DSF-A1	0.65
		DSF-B	16.59
Ein Gedi	31°30′N, 35°24′E	DSEn-C/A	20.05
		DSEn-B	18.96
Ze'elim	31°21′N, 35°24′E	DSZ-A	11.73
		DSZ-B	12.29
		DSZ-C	6.83
Hever	31°24′N, 35°23′E	DSH-A	4.47

METHODS

Field work and subsampling

The coring in the recent shore area was done with an Usinger piston corer (a modified Livingston piston corer) (Usinger 1991). The core sections are two meters long with diameters of 80 mm for the upper and 55 mm for the lower part of the cores. Back in the laboratory, the cores were cut into 1 m segments and split into halves. They were then sealed in polythene and stored at 4 °C.

The subsampling of the cores was performed in sampling intervals of about 2.5 cm with cubic plastic boxes (20 × 20 × 15 mm), which were pushed into the cleaned split surface of the core halves. Coarse grained sand layers were not subsampled. A first set of samples from the cores DSF-B, DSZ-A and -B and the uppermost 10 and 12 m of DSEn-C/A and -B, respectively, was taken in 2001. The surfaces of the core halves were partly covered with a brownish crust containing iron-oxides. The lowermost 10 and 8 m, respectively, of both cores from Ein Gedi were subsampled in the beginning of 2005, which is 4 yr later. Due to a high content of salt in the sediments the cores were still wet and not visibly alterated, except for the already mentioned surface oxidation. All samples were stored at 4°C in order to prevent them from drying. A total of 2763 samples were obtained

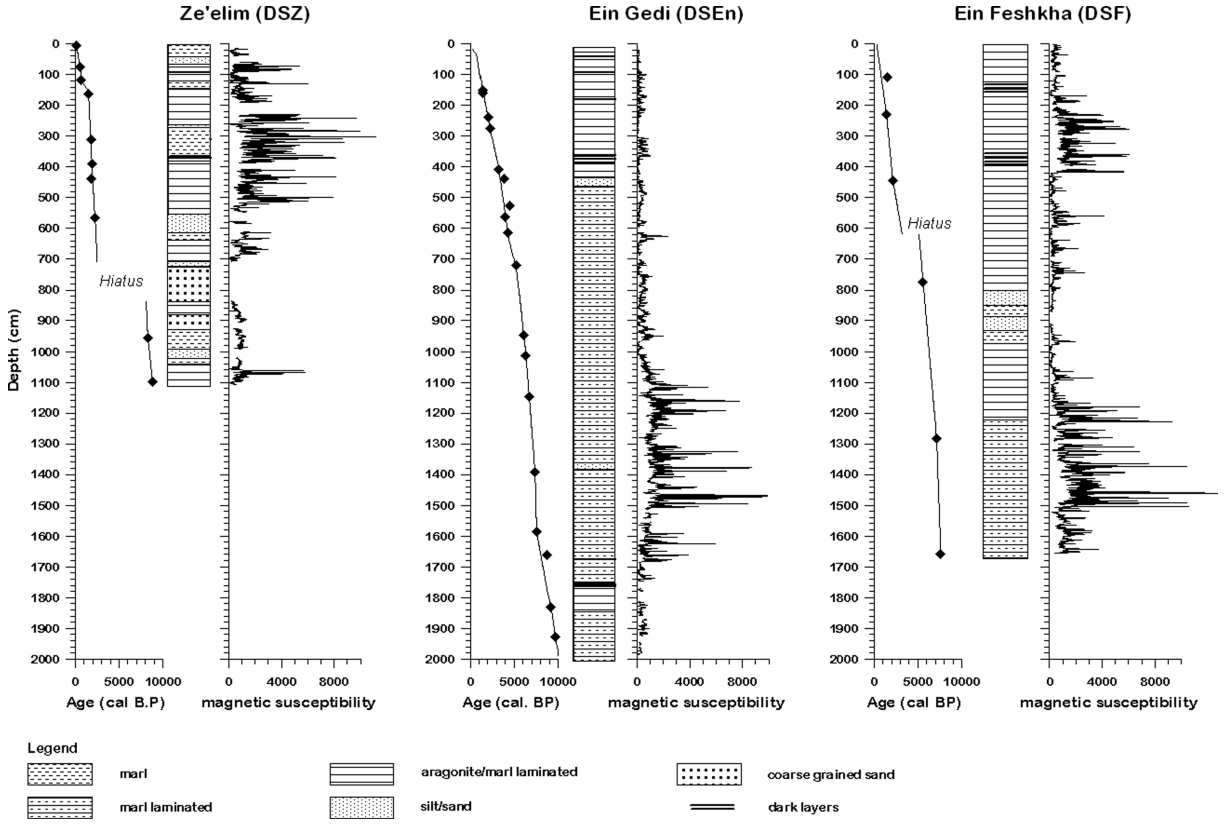

Figure 2. Depth/age models for the sediment profiles from Ze'elim, Ein Gedi and Ein Feshkha in combination with simplified lithological columns and the high resolution logs of magnetic susceptibility. The chronologies are based on calibrated AMS ^{14}C-ages measured on terrestrial plant remains (Migowski 2002). The error bars are smaller than the size of the symbols. The duration of the hiatuses are estimated on the basis of the extrapolated sedimentation rates.

from the five cores and 1723 out of these (cores DSF-B, DSZ-A and DSEn-C/A) were subjected to detailed rock magnetic investigations.

Chronology

The chronologies for the sediment profiles from the sites Ein Feskha, Ein Gedi and Ze'elim are based on AMS ^{14}C dating of terrestrial plant remains found within the sediment sequences (Migowski *et al.* 2004) (Fig. 2). Additional age information for the uppermost metres of the Ze'elim cores is available from correlation with the neighbouring outcrop in the Ze'elim gully (Ken-Tor *et al.* 2001; Migowski 2002). Although some of the radiocarbon dates did not fit well, the proposed depth-age models are in good agreement with the sediment structure, interpreting the medium to coarse grained sand layers in core DSZ-A (Figs 2 and 3a) as the onset of sedimentation after sedimentation breaks. Here two hiatuses spanning the time interval from 2.5 to 8 ka are located within a 2 m long section composed of coarse grained sand between 720 and 920 cm depth which is interrupted by a 30 cm thick sequence of laminated sediments. The latter could not be dated properly but is likely to be linked to a high stand of the Dead Sea level between 6 and 4.5 ka (Frumkin & Elitzur 2002; Migowski *et al.* 2006.). A hiatus with duration of about 3 kyr was identified within the sediment sequence of Ein Feshkha at about 620 cm depth (Figs 2 and 3c). The hiatus is located within a 15 cm thick sequence of deformed sediments that are interpreted as the result of erosion and reworking during a low stand of the Dead Sea water level associated with a dry period between 4 and 3.5 ka (Frumkin & Elitzur 2002). In this period the southern basin of the Dead Sea was completely dry.

Rock magnetic investigations

First of all, the magnetic susceptibility of the complete sediment profiles was continuously measured with a Bartington MS2E spot reading sensor in steps of 1 mm on the split halves of the cores directly after opening of the core tubes at the GeoForschungsZentrum Potsdam (GFZ) in 1998. The sensor is integrated in an automated core logging system designed at the Laboratory for Palaeo- and Rock Magnetism in Potsdam. Low-field magnetic susceptibility κ_{LF} of all the samples taken in 2001 was measured with an AGICO Kappabridge KLY-3S at 875 Hz. The intensities of the natural remanent magnetization (NRM) which will not be discussed here were measured with a fully automated 2G ENTERPRISES DC-SQUID 755 SRM long-core system with an in-line tri-axial degausser. Alternating field (AF-) demagnetization of the NRM was performed in 11 steps of up to 100 mT.

In order to obtain initial information about the magnetic properties of the heterogeneous sediments, the 16 m long core DSF-B from site Ein Feskha was then subjected to further detailed rock magnetic investigations. An anhysteretic remanent magnetization (ARM) was produced along the positive *z*-axis of the samples with 0.05 mT static field and 100 mT AF amplitude using a separate 2G ENTERPRISES 600 single-axis demagnetizer including an ARM-coil. The ARM intensities (J_{ARM}) where then measured and demagnetized with the 2G 755 SRM at AF levels of 0, 10, 20, 30, 40, 50, 65 and 80 mT. Isothermal remanent magnetizations (IRM) were imprinted with a 2G ENTERPRISES 660 pulse magnetizer and measured with a MOLYNEUX MiniSpin fluxgate magnetometer. Every 5th sample was exposed stepwise to peak fields of 5, 10, 15, 20, 50,

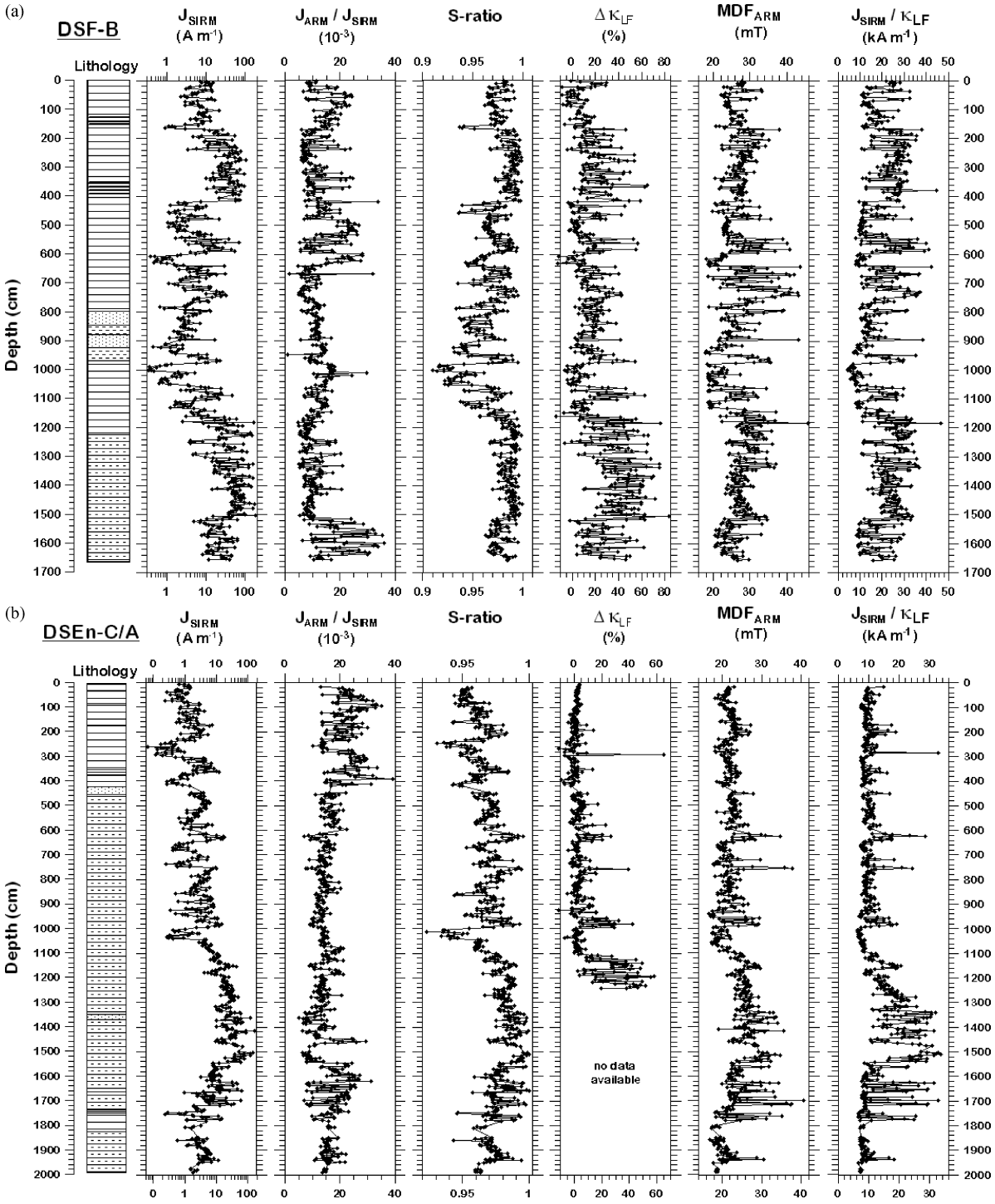

Figure 3. Simplified lithology, intensity of the saturation isothermal magnetization (SIRM) and records of parameters indicative for magnetic grain size, coercitivity and greigite content: ratio of the intensity of the anhysteretic remanent magnetization (J_{ARM})/J_{SIRM}, *S*-ratio, loss of magnetic susceptibility ($\Delta\kappa_{LF}$), median destructive field of the ARM (MDF_{ARM}) and ratio of J_{SIRM}/κ_{LF}, for (a) core DSF-B, (b) core DSEn-C/A and (c) core DSZ-A versus depth. *S*-ratio $= 0.5 \times (1 - SIRM_{1.5T}/IRM_{-0.3})$. Legends see Fig. 2.

100, 150, 200, 300, 450, 700, 1000 and 1500 mT along the positive *z*-axis of the samples in order to record complete IRM-acquisition curves. Because all pilot samples reached saturation between 300 and 1000 mT, a field of 1500 mT was chosen to imprint the saturation isothermal remanent magnetization (SIRM) of all other samples. *S*-ratios were calculated as $0.5 \times (1 - (IRM_{-0.3T}/SIRM_{1.5T}))$ following Bloemendal *et al.* (1992). A fully computer controlled variable field transition balance (VFBT), designed by Petersen, Munich, was used to measure the hysteresis parameter saturation magnetization (M_S), saturation remanence (M_{RS}), coercitivity force (H_C) and coercitivity of remanence (H_{CR}) and the temperature dependence of the saturation magnetization on a subset of samples. The samples were still wet at the beginning of the measurements.

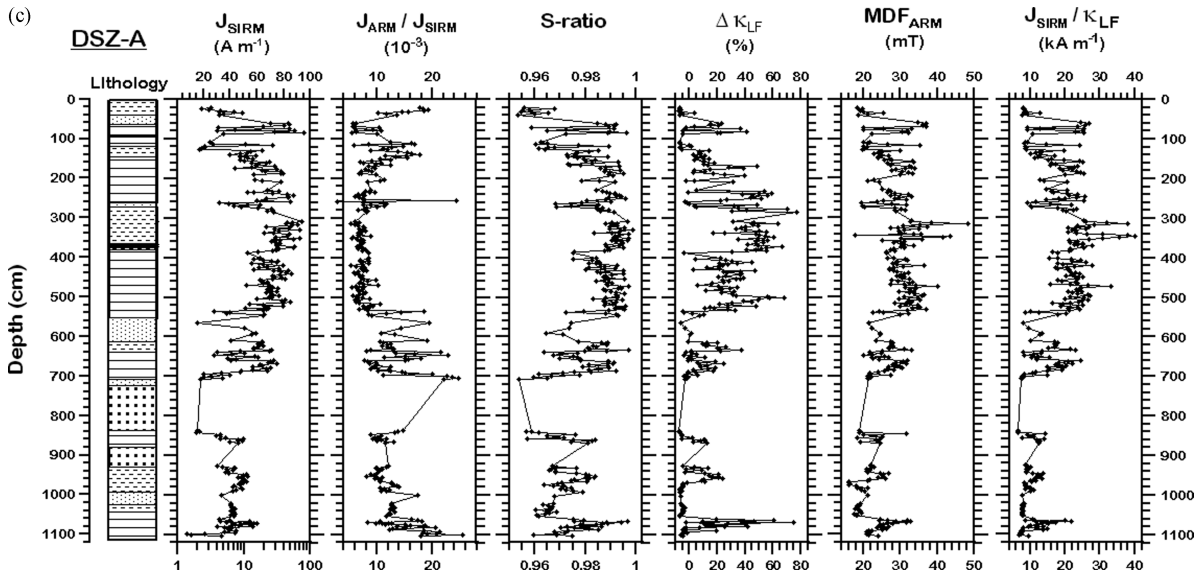

Figure 3. (*Continued.*)

Starting the new sampling campaign in 2005 in order to complete the palaeomagnetic profiles for the site Ein Gedi (Frank *et al.* 2007), rock magnetic parameters were additionally determined for cores DSZ-A and DSEn-C/A using the methods described above.

Cluster analysis

All rock magnetic parameters determined for cores DSF-B, DSEn-C/A and DSZ-A where subjected to a hierarchical agglomerative cluster analysis in order to separate the information on the variability of the different mineral magnetic phases in the sediment profiles from the Dead Sea into different groups. In order to ensure that the results obtained from the different cores are comparable to each other, cluster analysis was performed on the standard parameter set available for each sample, that is κ_{LF}, J_{ARM}, J_{SIRM}, median destructive field of the ARM (MDF_{ARM}) and NRM (MDF_{NRM}), *S*-ratio, ARM-susceptibility (κ_{ARM}) divided by κ_{LF}, ratio of J_{ARM}/J_{SIRM} and J_{SIRM} divided by κ_{LF}. The routine was performed with WinSTAT® for Excel (R. Fitch Software, 2003, http://www.winstat.de). Concentration dependent parameters vary over one or more orders of magnitude. Therefore, their logarithms were taken for statistical analysis. All rock magnetic parameters were then standardized yielding a variance of 1 and a mean value of 0. The Euclidean distance was computed and used as a measure of similarity between the pairs of data points. The agglomerations method used is based on the distance between the centres of gravity of the different groups.

The data set for core DSEn-C/A had to be divided into two parts that were separately analysed. This appeared to be necessary because half of the samples were cold stored for more than 3 yr before the rock magnetic investigations were performed whereas the other half was analysed immediately after sampling.

RESULTS AND DISCUSSION

Magnetic mineral concentration

The magnetic susceptibilities of all cores show strong variations, covering three orders of magnitude, reflecting the heterogeneous composition of the sediments. The latter is only partly seen in the simplified lithological columns (Fig. 2). In general the magnetic susceptibility in the sequences with finely laminated clastic material is higher than in the aragonite bearing sequences. The magnetic signal obtained from the cubic subsamples, however, is smoothed due to the lower resolution comprising layers with different magnetic characteristics within one sample which integrate over 2 cm. Amplitude variations in the records of J_{ARM} (not shown) and J_{SIRM} are identical to the susceptibility fluctuations (Figs 3a–c).

The concentration of magnetic minerals is highest in core DSZ-A from Ze'elim comprising the former near shore sediments (Fig. 3c). The nearby located Ze'elim River (Fig. 1) temporally transports clastic material into the Dead Sea, contributing additionally to the more clastic composition of this sequence, compared to Ein Feshkha, which is also a former near shore location. In the Ein Feshkha profile two defined intervals with higher magnetic concentration could be observed which corresponds to the time intervals 1.5–2 and 6.5–7.5 ka, respectively (Figs 2 and 3a), indicating a distinct change either in the level of the Dead Sea, the minerogenic components transported into the lake, or in the geochemical composition of the water body. The latter interval with higher susceptibilities is also visible in core DSEn-C/A from Ein Gedi (Figs 2 and 3b) which reflects the mostly undisturbed lacustrine succession. Here the increase in magnetic susceptibility is linked to a reduced occurrence of aragonite layers within the completely laminated sediment sequence.

Magnetic carrier minerals

As was suspected by the occurrence of dark layers within the sediment sequences there is a measurable amount of greigite still contributing to the sediment's remanence in all three profiles. The ratio of J_{SIRM}/κ_{LF}, a generally accepted greigite-indicative parameter (Hartstra 1982b; Snowball 1991; Roberts 1995; Dekkers & Schonen 1996), reaches peak values of up to 40 kA m^{-1} in intervals with a high concentration of magnetic minerals. In sedimentary sequences with magnetic susceptibility (SIRM) values $<500 \times 10^{-6}$ (10 A m^{-1}) the ratio J_{SIRM}/κ_{LF} is in the range of 10 kA m^{-1} (Figs 3a–c). Thus the increase in the concentration dependent parameters κ_{LF}

and J_{IRM} could not be interpreted as an increase in detritic influx alone, but also as a result of enhanced greigite formation.

Because the ratio of J_{SIRM}/κ_{LF} may also reflect grain size variations in case of pure (Ti-) magnetite assemblages, the loss of magnetic susceptibility during storage of the samples is an unambiguous proof for the former occurrence of greigite particles (Snowball & Thompson 1988). Therefore, we compared the results of the different magnetic susceptibility measurements performed during the last years. There is no real difference in the susceptibility values measured at the splitted core halves and the fresh samples (Fig. 4). This observation is valid not only for the samples taken in 2001 but also for the new sampling campaign in 2005 (Fig. 4). An error of at least ±5 per cent could be attributed to the sensitivity and calibration of the different instruments used. In contrast, the re-investigations of the samples from DSF-B, DSZ-A and the uppermost 12 m of DSEn-C/A stored for about 3 yr at 4°C and sealed into polythene sheets, revealed a loss of susceptibility ($\Delta\kappa_{LF}$) of up to 80 per cent (Figs 3a–c). The loss was highest in the samples with high SIRM-intensities and a J_{SIRM}/κ_{LF} ratio > 30 kA m^{-1}, that are the samples supposed to bear still high amounts of greigite. These

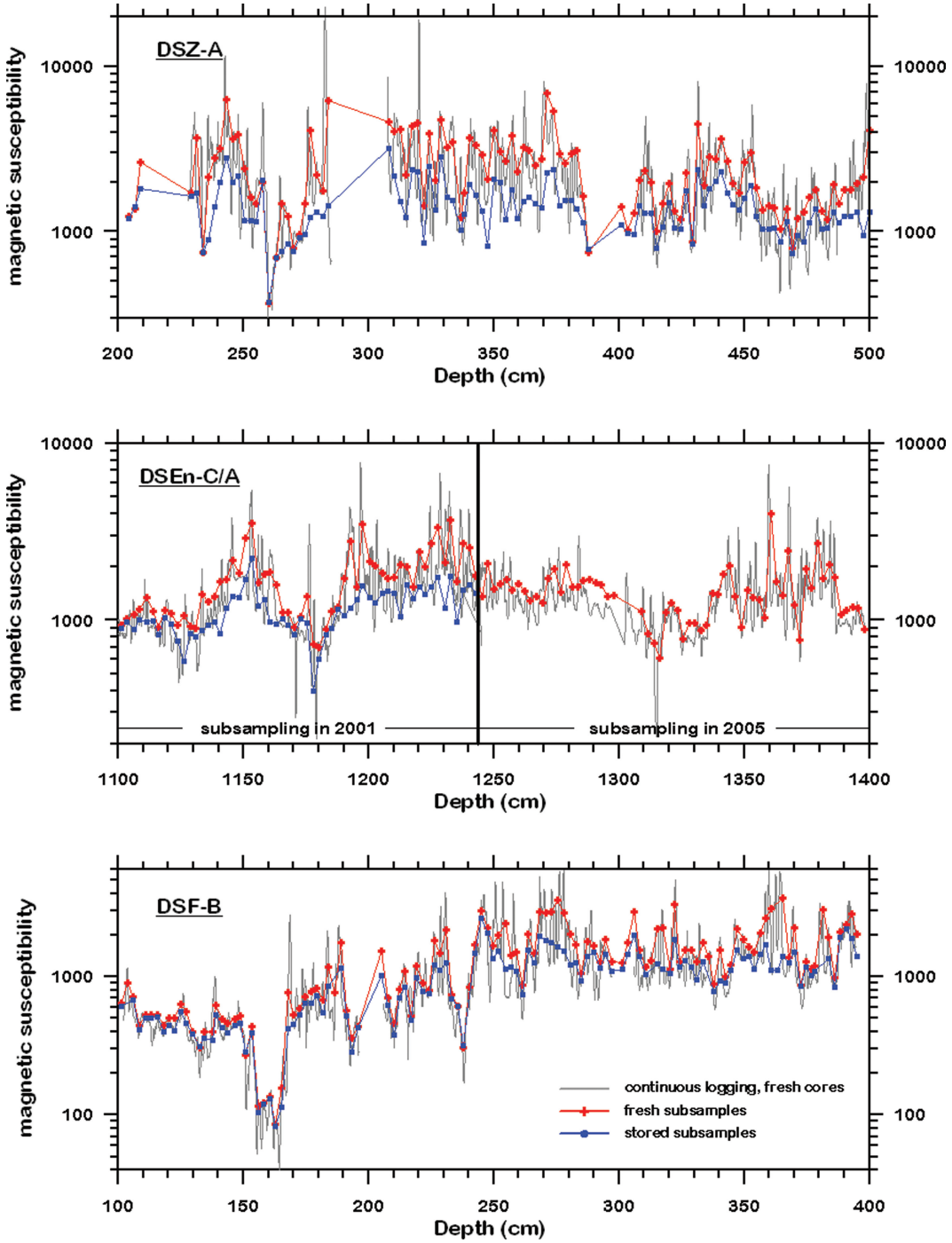

Figure 4. Comparison of the results from magnetic susceptibility measurements performed on the freshly splitted core halves (grey lines) and on the subsamples (red and blue lines) since 1998. For clarity of the figure only 4 m long intervals are shown from the three cores investigated. For further details see text.

samples are concentrated in the intervals from 150 to 400 cm and 1040 to 1660 cm in DSF-B (Fig. 3a), between 300 and 400 cm in core DSZ-A (Fig. 3c) and from 1340 to 1700 cm in DSEn-C/A (Fig. 3b). The corresponding time intervals are again 1.5–2 and 6.5–7.5 ka, indicating a major change in the geochemical conditions in the waterbody of the Dead Sea during these periods, linked to sea level fluctuations (Frumkin & Elitzur 2002; Bookman Ken-Tor *et al.* 2004).

High-temperature measurements of the saturation magnetization performed on samples from DSF-B revealed that a highly variable mixture of Ti-magnetite and Fe-sulphides controls the samples magnetizations (Fig. 5a). Typical heating curves show a distinct decrease in magnetization between 300 and 400°C, indicative for greigite (Snowball & Thompson 1990; Snowball 1991; Jelinowska *et al.* 1995; Roberts 1995) and a small tail caused by low-Ti magnetite, originating from the basalts in the catchment area of the Jordan River. The greigite decomposed during heating, the cooling curves show only the presence of low-Ti magnetite (Fig. 5a). High temperature runs on selected samples form the cores DSZ-A and DSEn-C/A yielded similar results (Fig. 6). The measurements were performed under helium or argon atmosphere but obviously there was still some oxygen left in the pulverized samples. The

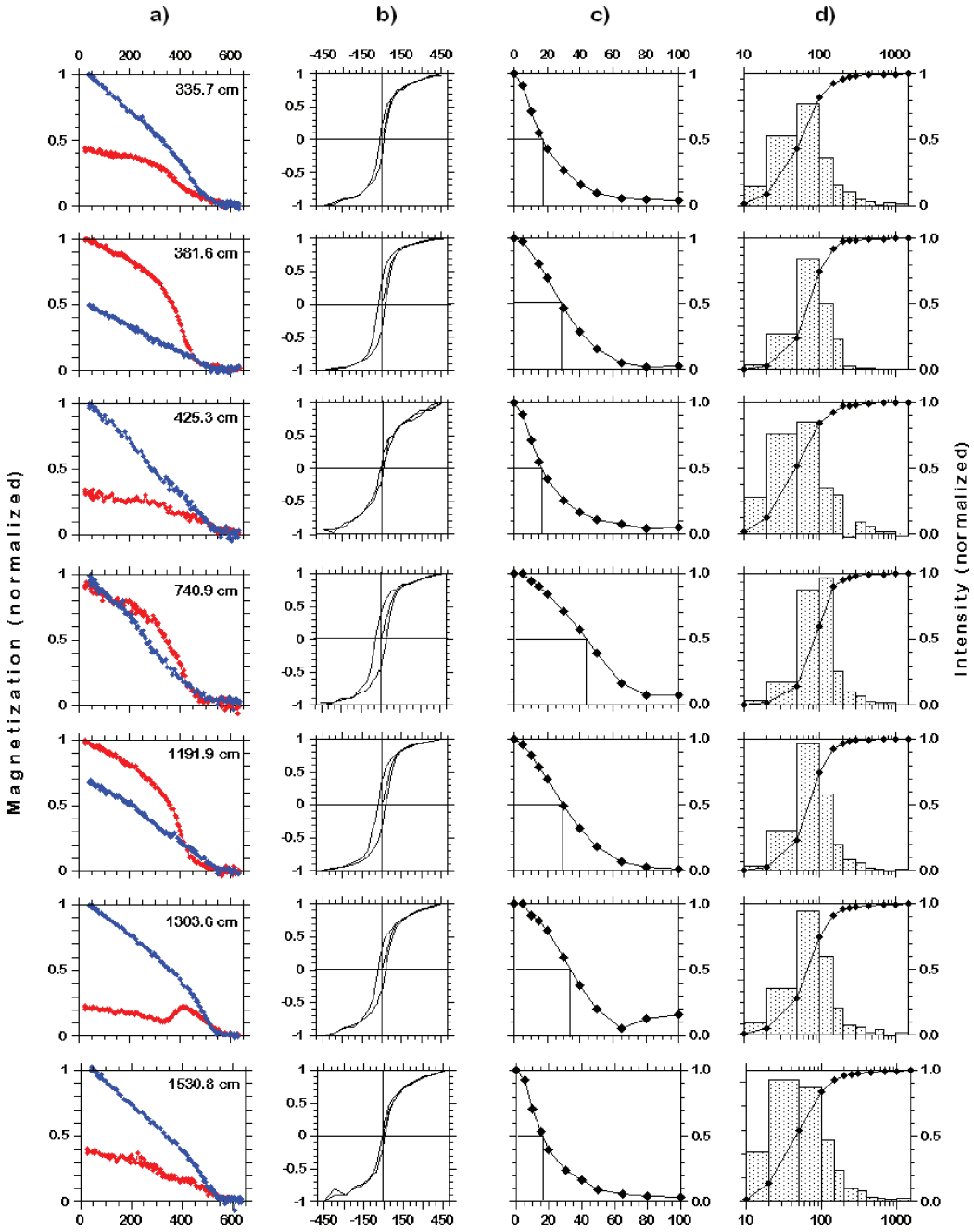

Figure 5. Identification of the magnetic carrier minerals in the sediments from Ein Feshkha by a combination of different methods: (a) temperature dependent measurements of the saturation magnetization, red diamonds denote the heating curves, blue diamonds the cooling curves; (b) hysteresis loops; (c) demagnetization curves of the natural remanent magnetization (NRM) and (d) acquisition curves of the IRM. The bar charts illustrate the variations in the IRM acquisition rate.

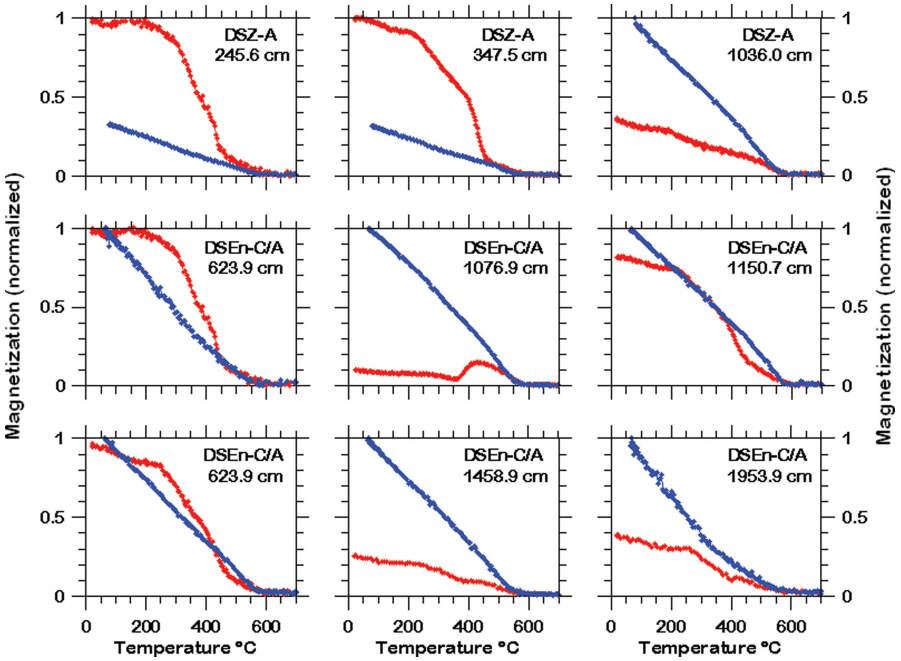

Figure 6. Temperature dependent measurements of the saturation magnetization of samples from cores DSEn-C/A and DSZ-A. Red diamonds denote the heating curves, blue diamonds the cooling curves.

formation of magnetite at temperatures from 340°C is mostly caused by high temperature oxidization of iron bearing paramagnetic minerals, most probably pyrite, and to an unmixing of maghemite Ti-magnetite intergrown. The occurrence of pyrite in the dark clastic layers was revealed by microscopical analysis (Migowski 2002). Maghemite and hematite were formed during weathering of the exposed basaltic rocks and are thought to contribute to the mineral magnetic fraction in small but varying amounts. The morphologies of the IRM-acquisition curves (Fig. 5d) also indicate that there is a more complex composition of the magnetic mineral fraction than just detrital low-Ti magnetite originating from Quaternary basalts and authigenic greigite alone.

Another hint for the presence of greigite would be the acquisition of a gyroremanent magnetization during AF demagnetization of the NRM at fields higher than 40 mT (Snowball 1997a,b; Hu *et al.* 1998; Sagnotti & Winkler 1999; Stephenson & Snowball 2001; Hu *et al.* 2002). However, this test failed nearly completely for the sediments from the Dead Sea (Fig. 5c). Sagnotti *et al.* (2005) indicated that sediments with a ratio of $J_{SIRM}/\kappa_{LF} < 20$ kA m^{-1} will not show significant gyromagnetic effects during AF demagnetization. In the sediments from the Dead Sea most of the samples have J_{SIRM}/κ_{LF}ratios between 10 and 20 kA m^{-1} (Figs 3a–c). The samples with values of J_{SIRM}/κ_{LF} up to 40 kA m^{-1} however, did also not necessarily acquire a GRM. This effect must probably be attributed to the composition of the sediment, differing distinctly from the sediments taken for GRM experiments. This assumption is corroborated by the results of a detailed analysis of the NRM-demagnetization curves revealing, that in the Dead Sea sediments a gyroremanenz is acquired in samples from disturbed sediment intervals rather than in those with high amounts of greigite (Frank *et al.* 2007).

Magnetic grain size and coercitivity dependent parameters

In sediments with (Ti-) magnetite as the dominant magnetic mineral, the variations in relative grain size are supposed to be reflected by the ratio of J_{ARM}/J_{SIRM} as well as by the coercitivity parameters MDF_{ARM} and *S*-ratio, since coarse grained MD (Ti-) magnetites have lower coercitivities than those in the SD-range (Hartstra 1982b). In the sediments from the Dead Sea the varying contributions of the different magnetic phases will certainly control the grain size indicative parameters. Nevertheless, the variations in the parameter J_{ARM}/J_{SIRM} and in the *S*-ratio follow the variations in concentration, here presented by J_{SIRM} (Figs 3a–c). A good example for this relation is given in the depth interval between 500 and 600 cm in core DSF-B (Fig. 3a). An increase in concentration is linked to an increase in grain size indicated by a decrease in J_{ARM}/J_{SIRM}, and corresponds to a decrease in the amount of higher coercive minerals, reflected by the parameter *S*-ratio. This observation would classically be interpreted as a result of an increased transport of detritic material into the lake, that is, a higher amount of coarse grained minerals. However, due to the presence of greigite, this interpretation is not straightforward, as it is shown by the variations in the coercitivity parameter MDF_{ARM}. These are contradictory to those in the *S*-ratio, indicating that the magnetic hardness increases when the content of higher coercive minerals decreases (Figs 3a–c). Additionally the MDF_{ARM} clearly parallels the greigite indicative parameter J_{SIRM}/κ_{LF}, indicating that a magnetic remanence carried by greigite is more resistant to AF-demagnetization than (Ti-) magnetite. This finding is corroborated by experimental results showing that the coercitivity spectrum of greigite spans higher values than those typical for (Ti-) magnetite (Roberts 1995; Dekkers & Schoonen 1996; Sagnotti & Winkler 1999).

Cluster analysis

In order to quantify the previous conclusions, the results from the cluster analysis performed on a set of rock magnetic parameters are shown as scatter-plots of different magnetic parameters in Fig. 7. Despite the differences in sediment composition between the three profiles, reflected in the magnetic concentration variations and

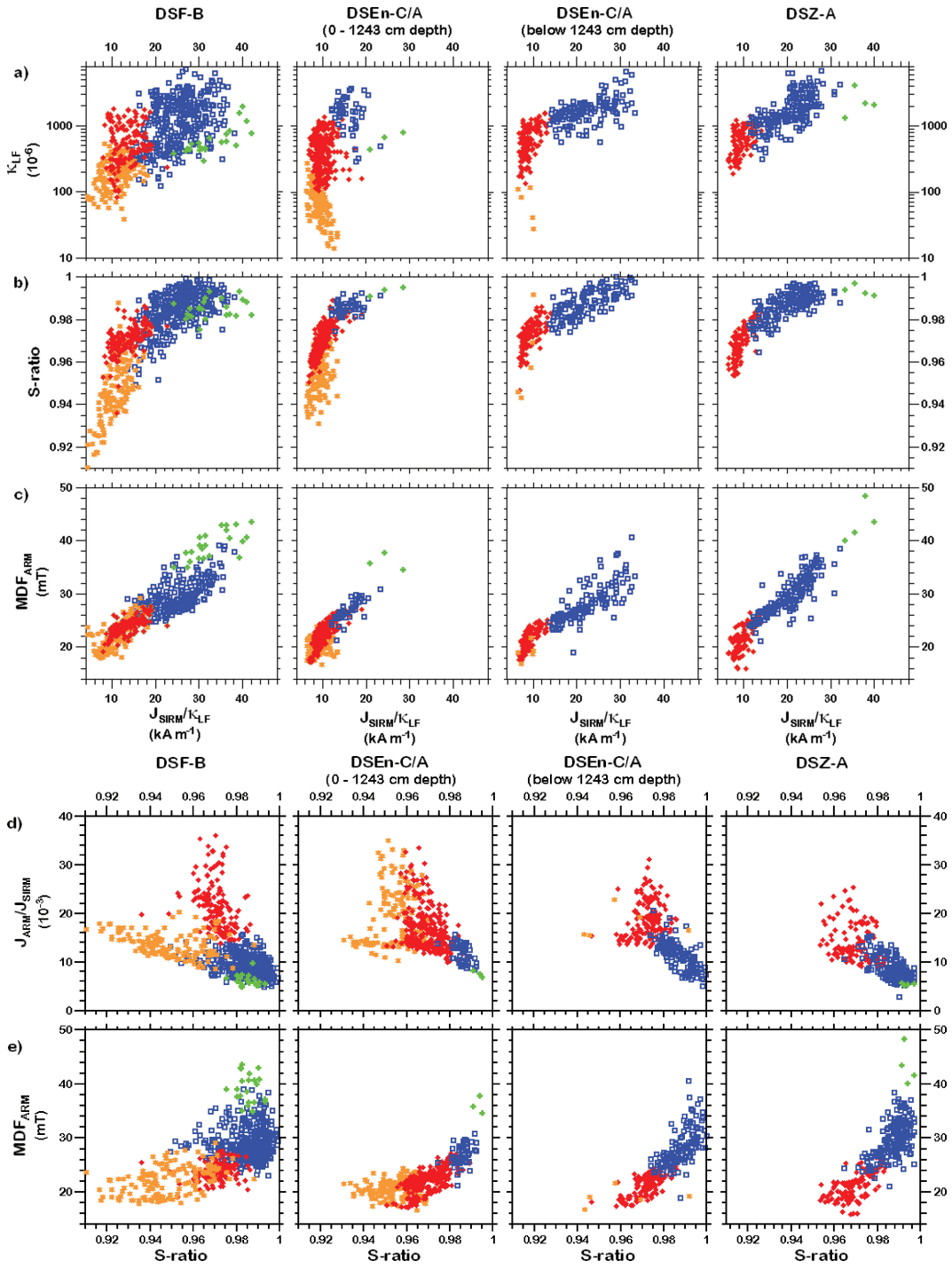

Figure 7. Estimating the relative portions of Ti-magnetite (T) and greigite (G) in the samples from DSF-B, DSEn-C/A and DSZ-A by combining different rock magnetic parameters indicative for coercitivity, grain size, magnetic concentration and greigite content in a series of scatter plots. The different coloured symbols correspond to the subdivision of the samples into four clusters as explained in the text. Green crosses: G $\gg$ T, blue squares: G $\geq$ T, red diamonds: G $\leq$ T, orange stars: G $\ll$ T.

absolute values (Figs 3a–c), the statistical analysis clearly yielded four clusters: two clusters which could be identified in each data set (red diamonds, blue squares) and two smaller groups of samples with more specific rock magnetic characteristics (orange stars, green crosses). A subdivision into more clusters would lower the comparability between the results of the different cores significantly. The boundaries of the clusters marked with the same colours in the individual cores differ from each other already, but they are still valid to group the variations in magnetic mineral composition in general.

The four clusters are obviously linked to the concentration variations, here presented by κ_{LF}, but they also seem to reflect the varying portions of authigenic Fe-sulphide and detrital Ti-magnetite in the samples (Fig. 7a). The samples that are supposed to contain high amounts of greigite are marked by green crosses in the bi-plots (Figs 7a–e). They were identified by their high ratios of

J_{SIRM}/κ_{LF} (>30 kA m^{-1}), which are typical for greigite bearing samples (Snowball 1991; Roberts 1995; Dekkers & Schonen 1996). Most of these samples, which have high, but not necessarily the highest, values of magnetic susceptibility, were found in core DSF-B and second, in DSZ-A, the nearshore cores (Fig. 7a). These samples are also characterized by the highest *S*-ratios between 0.98 and 1 (Fig. 7b), although the *S*-ratio of greigite should be lower compared to (Ti-) magnetite taking the differences in coercitivity (see above) in account. It was shown by Kruiver & Passier (2001) that the *S*-ratio reflects coercitivity variations within mixtures of magnetites originating either from magnetosomes or eolian dust, thus reflecting different grain sizes. *S*-ratios are highest when the coercitivity dispersion is small, that is saturation is more quickly achieved in fine grained magnetite with a narrow grain size distribution than in assemblages with higher amounts of coarser grained magnetites. This finding could obviously be transferred to the interpretation of the *S*-ratio in terms of greigite content, because authigenically formed greigite has smaller (single-domain (SD) range) grain sizes than detrital (Ti-) magnetite (pseudo-single (PSD) to multidomain (MD) range)(see Fig. 5b). The J_{ARM}/J_{SIRM} values for the greigite bearing samples are low ($< 10 \times 10^{-3}$) (Fig. 7d). In contrast, the MDF_{ARM} is distinctively higher (>34 mT) than it would be expected for coarse grained (Ti-) magnetite (5–15 mT, (Hartstra 1982a) (Figs 7c and e). This observation could probably be explained by the fact that a wider range of grain sizes fall within the SD-range for greigite compared to (Ti-) magnetite (Roberts 1995). In the lower part of core DSEn-C/A (>1243 cm) there are no samples belonging to the 'greigite cluster', the maximum J_{SIRM}/κ_{LF} value is 33 kA m^{-1} (Fig. 7a). However, there are some samples from the upper part of core DSEn-C/A (>1243 cm) that were grouped into this cluster, although their J_{SIRM}/κ_{LF} ratios are distinctively lower (Figs 7a–c). In this lacustrine sediment sequence the overall concentration of magnetic minerals is lower by a factor of ten compared to the cores from Ze'elim and Ein Feshkha (Fig. 2), so the samples containing greigite layers are obviously easier to identify.

The remaining samples form three clusters that differ from each other in the total amount of magnetic material on the one hand, and in the contribution of the different magnetic carrier minerals on the other hand (Figs. 7a). The latter is reflected in the values for *S*-ratio (Fig. 7b) and MDF_{ARM} (Fig. 7e). Samples marked by orange stars were obtained from sediment sections with a minor amount of detritic material. They have J_{ARM}/J_{SIRM} values in the range of 10 to 36×10^{-3}, *S*-ratios between 0.94 and 0.98, as well as MDF_{ARM} values below 28 mT (Figs 7d and e). The low MDF_{ARM} values in combination with the *S*-ratios indicate that this cluster contains samples with PSD to MD-Ti-magnetite with low to none contribution of greigite. The samples with *S*-ratios below 0.94 are supposed to include up to 10 per cent of high coercitive minerals like hematite, as it is corroborated by MDF_{ARM} values that are slightly higher than those of the neighboured samples with *S*-ratios >0.94 (Figs 7b and c).

The third group marked by red diamonds could then be interpreted in terms of a mixture of greigite and Ti-magnetite, where the latter are dominating the rock magnetic parameters. This group is characterized by high concentrations of magnetic minerals, *S*-ratios between 0.96 and 0.98, J_{ARM}/J_{SIRM} values between 10 to 36×10^{-3} and MDF_{ARM} between 16 and 28 mT (Fig. 7). These values correspond to those calculated for sediment samples from lake Birkat Ram, Israel, where only Ti-magnetites in the PSD-range are present (Frank *et al.* 2003). Therefore, it must probably be assumed that the red diamond cluster also contains samples with less to no contribution by greigite and that the difference between the red diamond and the orange star cluster is mainly caused by the differences in concentration (Fig. 7a).

The samples from the red diamond cluster overlaps with those from the cluster marked by blue squares. The latter are supposed to carry mixture of greigite and Ti-magnetite, too, but the greigite is dominating the magnetic behaviour (Figs 7a–e). Here the amount of greigite must be in the range of the Ti- magnetite at least but is probably up to four times higher for samples with J_{SIRM}/κ_{LF} > 20 kA m^{-1} (Fig. 7a). The magnetic carrier minerals were also recognized from *S*-ratios between 0.96 and 1.0 in combination with MDF_{ARM} values >24 mT and J_{ARM}/J_{SIRM} ratios $< 18 \times 10^{-3}$ (Figs 7c–e). There is obviously no remarkable contribution of higher coercive minerals like goethite or hematite to the magnetic mineral composition of the individual cores. These should be identified by low *S*-ratios (<0.9).

The quantitative estimation of the greigite content based on the interpretation of the cluster analysis corresponds to the results from the thermomagnetic measurements performed on the subset of samples presented in Figs 5(a) and 6. The samples that are characterized by a visible decrease in magnetization between 350 and 400 °C (Fig. 5a), fall within the two clusters containing samples with a major (blue squares) to dominant (green crosses) contribution by greigite. Samples showing a behaviour typical for sediments containing Ti-magnetite and paramagnetic minerals (425.3 and 1503.6 cm depth, Fig. 5a) belong to the clusters marked by orange stars and red diamonds, respectively.

An independent confirmation of the interpretation of the rock magnetic parameters in terms of varying greigite content is possible by adding the end members of the mixing lines suggested. These are either samples containing pure greigite or pure Ti-magnetite. The data set for the latter was taken from the investigation of sediments from Birkat Ram (Frank *et al.* 2003); a small crater lake located around 170 km north of the Dead Sea in the Golan Heights. The magnetic carrier minerals in the sediments are low Ti-magnetites that originate from volcanic rocks of Quaternary age in the catchment area. They should correspond to those transported into the Dead Sea by the Jordan River from the north, cutting through volcanic rocks of Quaternary age with a similar rock composition. The data sets for the greigite samples are from the investigation of (1) Cretaceous rocks from Alaska (Reynolds *et al.* 1994) and (2) hydrothermally synthesized greigite (Dekkers & Schoonen 1996). The comparison with the rock magnetic clusters obtained from core DSF-B, the most differentiated data set, is performed using again scatter plots (Figs 8a–d). The greigite samples are marked either by black diamonds (Cretaceous rocks, Reynolds *et al.* 1994) or black crosses (hydrothermally synthesized greigite Dekkers & Schoonen 1996), those containing Ti-magnetites are olive-coloured circles. Unfortunately, there is only one scatter-plot where both greigite data sets could be shown together (Fig. 8a); because not all rock magnetic parameters are available for both sets (Reynolds *et al.* 1994; Dekkers & Schoonen 1996).

The trends generated by the blue and green cluster (major to dominant contribution by greigite) are clearly continued by the pure greigite and greigite dominated rock samples (Fig. 8a). Additionally shown in Figs 8(a) and (d) are samples containing a mixture of greigite (G) and iron-titanium oxides (FT), also taken from Reynolds *et al.* (1994). Closed grey diamonds denote samples with G > FT and open grey diamonds those with G < FT. The first ones show a rock magnetic behaviour very similar to those identified as 'dominated by greigite' in the Dead Sea sediments (green crosses). The small offset between the two group of samples that are described as greigite dominated (green crosses, closed grey diamonds) could either be

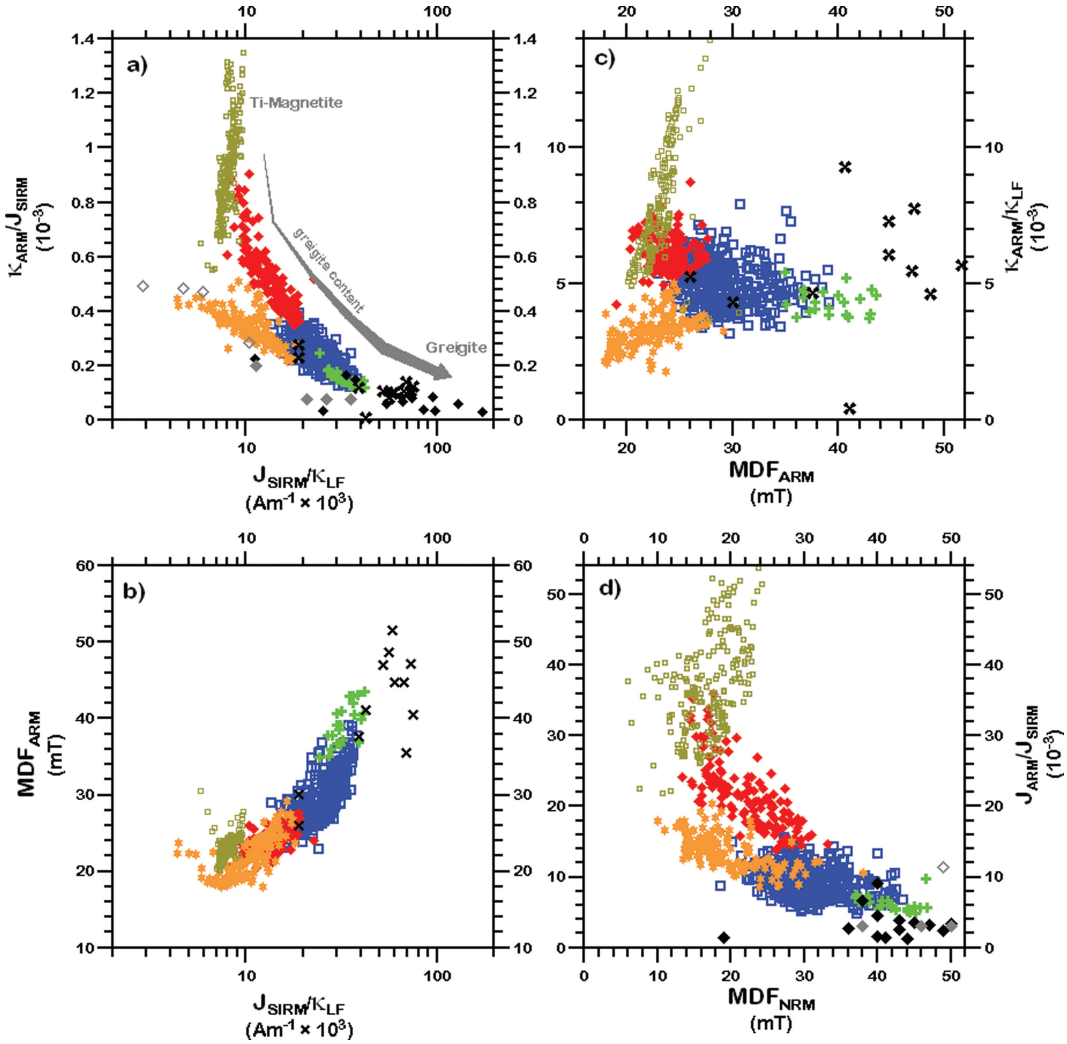

Figure 8. Comparison of the results from the cluster analysis for core DSF-B, interpreted in terms of varying greigite content, together with published data for greigite (black diamonds, black crosses) (Reynolds *et al.* 1994; Dekkers & Schoonen 1996) and low Ti-magnetite (Frank *et al.* 2003) (olive dots). Additionally, shown are samples containing mixtures of greigite (G) and iron-titanium oxides (FT), also taken from Reynolds *et al.* (1994). Closed grey diamonds denote samples with G > FT and open grey diamonds those with G < FT.

attributed to the lithogenic differences, that is the composition of the sediment matrix, sediment structure, occurrence/type of diagenesis, or to the different experimental procedures used to imprint the ARM (Sagnotti *et al.* 2003).

Based on the scatter plots the interpretation for the clusters marked by orange stars and red diamonds could be improved (Figs 8a–d). They were interpreted as samples with PSD to MD-Ti-magnetites with less to no contribution of greigite, separated on the base of the remarkable differences in concentration. However, the comparison with the data set from Birkat Ram reveals, that the samples marked by orange stars are those with a low greigite content and low concentration, whereas the red diamond group contains also the samples with Ti-magnetite only (Figs 8a and c). Naturally there is some overlapping, but the differentiation becomes quite clear especially in plotting J_{SIRM}/κ_{LF} versus κ_{ARM}/J_{SIRM}(Fig. 8a). The samples from the cretaceous rocks with G < FT (open grey diamonds) and G > FT (closed grey diamonds) fit perfectly into the mixing trend given by the orange star, blue square and green cross clusters, corroborating the decrease in greigite content expressed by the decrease in J_{SIRM}/κ_{LF} and an increase in J_{ARM}/J_{SIRM} (Fig. 8a). The content of Ti-magnetite must be constantly low in these samples in order to allow for such an interpretation. The trend expressed by the samples that have a major contribution by greigite (blue squares) in combination with the red diamond cluster could than be interpreted as an increase in the amount of Ti-magnetites and a concurrent decrease of greigite minerals until there is none of the latter at all. These are the samples which have similar rock magnetic characteristics like the low Ti-magnetite samples from Birkat Ram (olive circles).

Essentially the interpretation made above could be applied to the results obtained from cores DSEn-C/A and DSZ-A also (Fig. 9). The differentiation between the red diamond and the orange star cluster however is not as striking as in core DSF-B. This is due to different reasons. First of all, the cluster analysis performed for cores DSZ-A did not reveal any sample for the orange star cluster. Second, there are not enough samples for the lowermost part of DSEn-C/A to define the orange star cluster properly (Figs 7a–e). Third, the uppermost 1243 cm long sediment sequence of core DSEn-C/A has a quite different sediment composition with a much lower magnetic mineral concentration compared to the sediments from Ein Feshkha

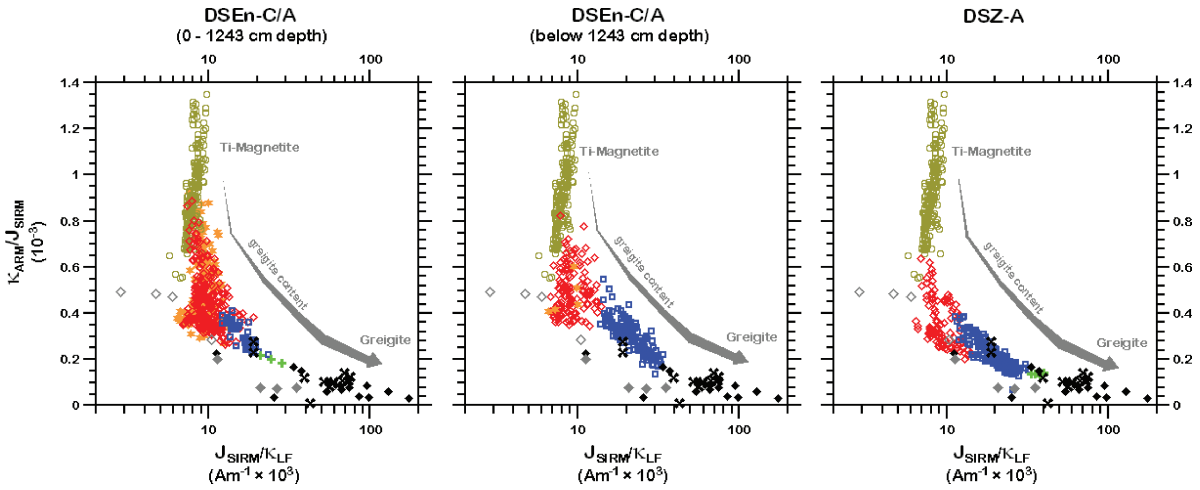

Figure 9. Comparison of the results of the cluster analysis obtained for core DSEn-C/A and DSZ-A with published data for greigite (black diamonds, black crosses) (Reynolds *et al.* 1994; Dekkers & Schoonen 1996) and low Ti-magnetite (Frank *et al.* 2003) (olive dots). Additionally shown are samples containing mixtures of greigite (G) and iron-titanium oxides (FT), also taken from Reynolds *et al.* (1994). Closed grey diamonds denote samples with G > FT and open grey diamonds those with G < FT.

(Fig. 2). The orange star cluster calculated for the top part of DSEN-C/A includes samples with susceptibility values in a range that is not represented in DSF-B (Fig. 7a). Therefore, the major part of these samples did not fit into the presented interpretation scheme but have magnetic characteristics very similar to the samples marked by red diamonds, but with a lower magnetic concentration.

Hysteresis loop measurements

The results of the hysteresis loop measurements performed on a subset of samples from core DSF-B are presented in Fig. 10. Some

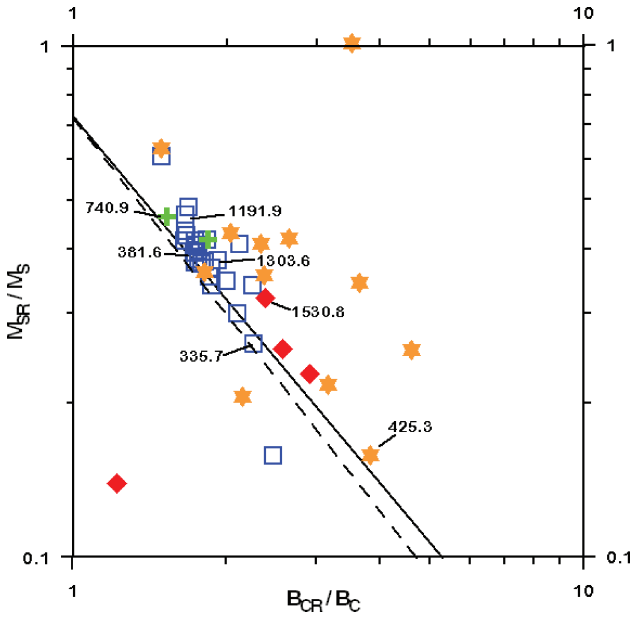

Figure 10. Results from hysteresis measurements carried out on 51 samples from core DSF-B presented in a logarithmically scaled Day plot (Day *et al.* 1977). The different symbols correspond to the subdivision of the samples into four clusters as shown in Fig. 7. For further details see Fig. 7 and text. The samples identified by their depth are the same as presented in Fig. 5. Additionally shown are the mixing lines for sedimentary greigite samples from Roberts (1995) (solid line) and Jelinowska *et al.* (1998) (dashed line).

of the corresponding hysteresis loops are shown in Fig. 5(b). The colour coding is the same as was chosen for the cluster analysis. Most of the samples characterized by high greigite contents (green crosses, blue squares) have B_{CR}/B_C ratios between 1.5 and 1.9 and M_{SR}/M_S ratios of 0.36–0.51 (Fig. 10). These values correspond to those obtained from rock magnetic investigations of sedimentary greigite (Roberts 1995). The samples from the same cluster but with lower M_{SR}/M_S ratios and higher B_{CR}/B_C ratios are supposed to contain less greigite. This interpretation is strongly supported by the results of Roberts (1995) and Jelinowska *et al.* (1998) who calculated mixing lines out of their results of hysteresis loop measurements performed on natural and synthetic greigite samples. Most of the samples marked either by green crosses or blue squares are lying on or near these lines (Fig. 10). The cluster of these samples overlaps with that of samples dominated by Ti-magnetite and a low to no contribution by greigite (red diamonds, orange stars, Fig. 8). Only a few of these samples cluster in a defined area of the Day-diagram most of them are rather widely distributed. This must be attributed to the fact that (1) at least one third of the samples marked by red diamonds are characterized by low J_{ARM}/J_{SIRM} ratios and low MDF_{ARM} indicating the presence of coarse grained Ti-magnetite and (2) most of the samples from the orange star cluster have a low magnetic mineral concentration resulting in noisy hysteresis loops.

It is not possible to obtain any information on the domain state of the magnetic particles using the Day-plot which is only valid for pure (Ti-) magnetites. There is also no possibility to estimate the relative grain size of the greigite based on the presented results.

CONCLUSION

The detailed rock magnetic investigations performed on samples from the lacustrine sediments of the Dead Sea, Israel, revealed that Ti- magnetite and greigite are the main magnetic carrier minerals in these sediments. As indicated by the high temperature runs of the saturation magnetization the concentration of both magnetic fractions is highly variable throughout the profiles. Results of a cluster analysis presented within scatter plots of different rock magnetic parameters allow for a qualitative estimation of the amount of greigite in the various samples. These were divided into four groups, which

are (1) dominated by greigite, have (2) a high and (3) a low greigite content or have (4) low to no contribution by greigite. The differentiation between the two last-named groups is not valid for all three profiles because of the differences in sediment composition. Additionally it has to be considered that the boundaries between the different clusters are not well defined in all cases. Nonetheless, the results of the qualitative greigite estimation are confirmed by the comparison of the rock magnetic characteristics with those known for greigite and greigite dominated rock samples and low Ti-magnetite samples, taken from the literature. The samples from the Dead Sea are distributed along a mixing line between the end members greigite and low Ti-magnetite. An interpretation of the rock magnetic results in terms of grain size variation is not possible, but the hysteresis loop measurements revealed that the greigite shows SD-behaviour. The combination of the commonly accepted greigite indicative parameter J_{SIRM}/κ_{LF} with those normally interpreted in terms of grain size or coercitivity variations in monomineralic (Ti-) magnetites magnetic fractions yielded information about rock magnetic parameter values typical for greigite bearing samples. Low values for the grain size dependent parameters κ_{ARM}/J_{SIRM} or J_{ARM}/J_{SIRM} are linked to high amounts of greigite and vice versa. The MDFs of the ARM and the NRM for samples dominated by greigite are >30 mT, because the coercitivity of greigite is slightly higher than of (Ti-) magnetites. Another parameter found to be suitable for the identification of greigite is the *S*-ratio which is near 1 for greigite dominated samples.

ACKNOWLEDGMENTS

The authors wish to thank J. Mingram, D. Berger, M. Köhler and M. Prena for coring and H. Lippitz and C. Schmeltzer for help during laboratory work. H. Ron is acknowledged for the discussions on the rock magnetic results. M. Stein contributed to the organization of the drilling campaign. L. Sagnotti and P. Vlag are kindly acknowledged for their very helpful review comments. This study was funded by the German Research Foundation (DFG), grant Ne 154/37-1.

REFERENCES

Bloemendal, J., King, J.W., Hall, F.R. & Doh, S.-J., 1992. Rock magnetism of late Neogene and Pleistocene deep-sea sediments: Relationship to sediment source, diagenetic processes, and sediment lithology, *J. geophys. Res.,* **97,** 4361–4375.

Bookman (Ken-Tor), R., Enzel, Y., Agnon, A. & Stein, M., 2004. Late Holocene lake levels of the Dead Sea, *GSA Bulletin,* **116,** 555–571.

Day, R., Fuller, M. & Schmidt, V.A., 1977. Hysteresis properties of titanomagnetites: grain size and compositional dependence, *Phys. Earth planet. Int.,* **13,** 260–267.

Dekkers, M.J. & Schoonen, M.A.A., 1996. Magnetic properties of hydrothermally synthesized greigite (Fe_3S_4)—II. Rock magnetic parameters at room temperature, *Geophys. J. Int.,* **126,** 360–368.

Dunlop, D.J.& Özdemir, Ö. , 1997. *Rock Magnetism—Fundamentals and frontiers*, Cambridge University Press, Cambridge, p. 573.

Frank, U., Nowaczyk, N.R., Negendank, J.F.W. & Melles, M., 2002. A paleomagnetic record from Lake Lama, northern Central Siberia, *Phys. Earth planet. Int.,* **133,** 3–20.

Frank, U., Schwab, M.J. & Negendank, J.F.W., 2003. Results of rock magnetic investigations and relative paleointensity determinations on lacustrine sediments from Birkat Ram, Golan Heights (Israel).,*J. geophys. Res.,* **108,** doi:10.1029/2002JB002049.

Frank, U., Nowaczyk, N.R. & Negendank, J.F.W., 2007. Palaeomagnetism of greigite bearing sediments from the Dead Sea, Israel, *Geophys. J. Int.,* doi:10.1111/j.1365-246X.2006.03263.x

Frumkin, A. & Elitzur, Y., 2002. Historic Dead Sea level fluctuations calibrated with geological and archaeological evidence, *Quat. Res.,* **57,** 3, 334–342.

Garfunkel, Z. & Ben-Avraham, Z., 1996. The structure of the Dead Sea basin, *Tectonophysics,* **266,** 155–176.

Geiss, C.E. & Banerjee, S.K., 1997. A multi-parameter rock magnetic record of the last glacial-interglacial paleoclimate from south-central Illinois, USA, *Earth planet. Sci. Lett.,* **152,** 203–216.

Geiss, C.E. & Banerjee, S.K., 2003. A Holocene-Late Pleistocene geomagnetic inclination record from Grandfather Lake, SW Alaska, *Geophys. J. Int.,* **153,** 497–507.

Hartstra, R.L., 1982a. A comparative study of the ARM and I_{SR} of some natural magnetites of MD and PSD grain size, *Geophys. J. R. astr. Soc.,* **71,** 497–518.

Hartstra, R.L., 1982b. Grain size dependence of initial susceptibility and saturation magnetization related parameters of four natural magnetites in the PSD-MD range, *Geophys. J. R. astr. Soc.,* **71,** 477–495.

Hassan, M.A. & Klein, M., 2002. Fluvial adjustment of the lower Jordan River to a drop in the Dead Sea level, *Geomorphology,* **45,** 21–33.

Hirt, A.M., Lanci, L. & Koinig, K., 2003. Mineral magnetic record of Holocene environmental changes in Sägistalsee, Switzerland, *J. Paleolim.,* **30,** 321–331.

Hu, S., Appel, E., Hoffmann, V., Schmahl, W.W. & Wang, S., 1998. Gyromagnetic remanence acquired by greigite (Fe_3S_4) during static three-axis alternating field demagnetization, *Geophys. J. Int.,* **134,** 831–842.

Hu, S., Stephenson, A. & Appel, E., 2002. A study of gyroremanent magnetisation (GRM) and rotational remanent magnetisation (RRM) carried by greigite from lake sediments, *Geophys. J. Int.,* **151,** 469–474.

Jansa, J., Novák, F. & Stastný, M., 1998. Greigite from the sediments in the Most Basin (Czech Republic), *Vestnik Ceského geologickéhotístavu,* **73,** 85–88.

Jelinowska, A., Tucholka, P., Gasse, F. & Fontes, J.C., 1995. Mineral magnetic record of environment in Late Pleistocene and Holocene sediments, Lake Manas, Xinjiang, China, *Geophys. Res. Lett.,* **22,** 953–956.

Jelinowska, A. et al., 1998. Mineral magnetic study of Late Quaternary South Caspian Sea sediments: palaeoenvironmental implications, *Geophys. J. Int,* **133,** 499–509.

Ken-Tor, R., Agnon, A., Enzel, Y., Stein, M., Marco, S. & Negendank, J.F.W., 2001. High-resolution geological record of historic earthquakes in the Dead Sea basin, *J. geophys. Res.,* **106,** 2221–2234.

Kruiver, P.P. & Passier, H.P., 2001. Coercitivity analysis of magnetic phases in sapropel S1 related to variations in redox conditions, including an investigation on the S ratio, *Geochem. Geophys. Geosyst.,* **3,** doi:2001GC000181.

Maher, B.A. & Thompson, R., 1999. *Quaternary Climates, Environments and Magnetism*, Cambridge University Press, Cambridge, p. 390.

Migowski, C., 2002. Untersuchungen laminierter holozäner Sedimente aus dem Toten Meer: Rekonstruktion von Paläoklima und -seismizität, *Scientific Technical Reports* **02/06,** Potsdam, 99 pp.

Migowski, C., Ken-Tor, R., Negendank, J.F.W., Stein, M. & Mingram, J., 1998. Post-Lisan record documented in sediment sequences from the western shore area and the central basin of the Dead Sea, *TerraNostra,* **98/6,** 100–102.

Migowski, C., Stein, M., Prasad, S., Negendank, J.F.W. & Agnon, A., 2006. Holocene climate variability and cultural evolution in the Near East from the Dead Sea sedimentary record, *Quat. Res.,* **66,** 3, 421–431.

Migowski, C., Agnon, A., Bookman, R., Negendank, J.F.W. & Stein, M., 2004. Recurrence pattern of Holocene earthquakes along the Dead Sea transform revealed by varve-counting and radiocarbon dating of lacustrine sediments, *Earth planet. Sci. Lett.,* **222,** 301–314.

Nissenbaum, A. & Kaplan, I.R., 1976. Sulfur and carbon isotopic evidence for biogeochemical processes in the Dead Sea ecosystem, in *Carbon, nitrogen, phosphorus, sulfur and selenium cycles*, pp. 309–325, ed. Nriagu, J.O., Ann Arbor Science Publishers, Ann Arbor, MI, USA.

Reynolds, R.L., Tuttle, M.L., Rice, C.A., Fishman, N.S., Karachewski, J.A. & Sherman, D.M., 1994. Magnetization and geochemistry of greigite-bearing cretaceous strata, North Slope Basin, Alaska, *Am. J. Sci.,* **294,** 485–528.

Reynolds, R.L., Rosenbaum, J.G., van Metre, P., Tuttle, M., Callender, E. & Goldin, A., 1999. Greigite (Fe^3S^4) as an indicator of drought—The 1912–1994 sediment magnetic record from White Rock Lake, Dallas, Texas, USA, *J. Paleolim.,* **21,** 193–206.

Roberts, A.P., 1995. Magnetic properties of sedimentary greigite (Fe_3S_4), *Earth planet. Sci. Lett.,* **134,** 227–236.

Roberts, A.P. & Turner, G.M., 1993. Diagenetic formation of ferrimagnetic iron sulphide minerals in rapidly deposited marine sediments, South Island, New Zealand, *Earth planet Sci. Lett.,* **115,** 257–273.

Roberts, A.P. & Weaver, R., 2005. Multiple mechanism of remagnetization involoving sedimentary greigite (Fe^3S^4), *Earth planet. Sci. Lett.,* **231,** 263–277.

Rolph, T.C., Vigliotti, L. & Oldfield, F., 2004. Mineral magnetism and geomagnetic secular variation of marine and lacustrine sediments from central Italy: timing and nature of local and regional Holocene environmental change, *Quat. Sci. Rev.,* **23,** 1699–1722.

Sagnotti, L. & Winkler, A., 1999. Rock magnetism and palaeomagnetism of greigite-bearing mudstones in the Italian peninsula, *Earth planet. Sci. Lett.* **165,** 67–80.

Sagnotti, L., Rochette, P., Jackson, M., Vadeboin, F., Dinarès-Turell, J., Winkler, A. & 'Mag-Net', Science Team, 2003. Inter-laboratory calibration of low-field magnetic and anhysteretic susceptibillity measurements, *Phys. Earth planet. Int.,* **138,** 25–38.

Sagnotti, L.. Roberts, A.P., Weaver, R., Verosub, K.L., Florindo, F., Wilson, G.S., Pike, C.R. & Clayton, T., 2005. Apparent high-frequency magnetic polarity reversals due to alternating remagnetization resulting from late diagenetic growth of greigite from siderite, *Geophys. J. Int.,* **129,** 89–100.

Snowball, I. & Thompson, R., 1988. The occurrence of greigite in sediments from Loch Lomond, *J. Quat. Sci.,* **3,** 121–125.

Snowball, I. & Thompson, R., 1990. A stable chemical remanence in Holocene sediments, *J. geophys. Res.,* **95,** 4471–4479.

Snowball, I.F., 1991. Magnetic hysteresis properties of greigite (Fe_3S_4) and a new occurrence in Holocene sediments from Swedish Lappland, *Phys. Earth planet. Int.,* **68,** 32–40.

Snowball, I.F., 1997a. Gyroremanent magnetization and the magnetic properties of greigite-bearing clays in southern Sweden, *Geophys. J. Int.,* **129,** 624–636.

Snowball, I.F., 1997b. The detection of single-domain greigite (Fe_3S_4) using rotational remanent magnetization (RRM) and the effective gyro field (*Bg*): mineral magnetic and paleomagnetic applications, *Geophys. J. Int.* **130,** 704–716.

Stephenson, A. & Snowball, I., 2001. A large gyromagnetic effect in greigite, *Geophys. J. Int.,* **145,** 570–575.

Strechie, C., André, F., Jelinowska, A., Tucholka, P., Guichard, F., Lericolais, G. & Panin, N., 2002. Magnetic minerals as indicators of major environmental change in Holcene Black Sea sediments: preliminary results, *Phys. Chem. Earth,* **27,** 1363–1370.

Usinger, H., 1991. Ein Stechbohrgerät zum Bergen von Torfen und Seesedimenten für Einsatz bis zu größeren Tiefen, in *Symposium on Palaeolimnology of Maar Lakes*, p. 55, eds Zolitschka, B. & Negendank, J.F.W., Bitburg.

Vlag, P., Thouveny, N., Williamson, D., Andrieu, V., Icole, M. & Velzen, A.J.v., 1997. The rock magnetic signal of climate change in the maar lakes sequence of Lac St Front (France), *Geophys. J. Int.,* **131,** 724–740.

Wang, H., Liu, H., Cui, H. & Abrahamsen, N., 2001. Terminal Pleistocene/Holocene palaeoenvironmantal changes revealed by mineral-magnetism measurements of lake sediments for Dali nor area, southeastern Inner Mongolia Plateau, China, *Paleo, Paleo, Paleo,* **170,** 115–132.

Yamazaki, T., Abdeldayem, A.L. & Ikehara, K., 2003. Rock-magnetic changes with reduction diagenesis in Japan Sea sediments and preservation of geomagnetic secular variation in inclination during the last 30,000 yr, *Earth Planets Space,* **55,** 327–340.